ACCOUNTS
of chemical research

Mechanisms of Single-Walled Carbon Nanotube Nucleation, Growth, and Healing Determined Using QM/MD Methods

ALISTER J. PAGE,[†] YASUHITO OHTA,[‡] STEPHAN IRLE,[*,§] AND KEIJI MOROKUMA[*,†,∥]

[†]*Fukui Institute for Fundamental Chemistry, Kyoto University, Kyoto 606-8103, Japan,* [‡]*Department of Chemistry, Nara Women's University, Nara 630-8506, Japan,* [§]*Institute for Advanced Research and Department of Chemistry, Nagoya University, Nagoya 464-8602, Japan, and* [∥]*Cherry L. Emerson Center for Scientific Computation and Department of Chemistry, Emory University, Atlanta, Georgia 30322*

RECEIVED ON APRIL 16, 2010

Ⓦ This paper contains enhanced objects available on the Internet at http://pubs.acs.org/acr.

CONSPECTUS

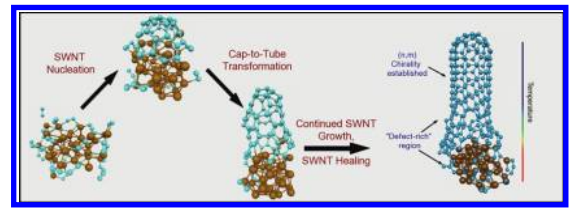

Since their discovery in the early 1990s, single-walled carbon nanotubes (SWNTs) have spawned previously unimaginable commercial and industrial technologies. Their versatility stems from their unique electronic, physical/chemical, and mechanical properties, which set them apart from traditional materials.

Many researchers have investigated SWNT growth mechanisms in the years since their discovery. The most prevalent of these is the vapor−liquid−solid (VLS) mechanism, which is based on experimental observations. Within the VLS mechanism, researchers assume that the formation of a SWNT starts with co-condensation of carbon and metal atoms from vapor to form liquid metal carbide. Once the liquid reaches supersaturation, the solid phase nanotubes begin to grow. The growth process is partitioned into three distinct stages: nucleation of a carbon "cap-precursor," "cap-to-tube" transformation, and continued SWNT growth. In recent years, molecular dynamics (MD) simulations have come to the fore with respect to SWNT growth. MD simulations lead to spatial and temporal resolutions of these processes that are superior to those possible using current experimental techniques, and so provide valuable information regarding the growth process that researchers cannot obtain experimentally.

In this Account, we review our own recent efforts to simulate SWNT nucleation, growth, and healing phenomena on transition-metal catalysts using quantum mechanical molecular dynamics (QM/MD) methods. In particular, we have validated each stage of the SWNT condensation mechanism using a self-consistent-charge density-functional tight-binding (SCC-DFTB) methodology. With respect to the nucleation of a SWNT cap-precursor (stage 1), we have shown that the presence of a transition-metal carbide particle is not a necessary prerequisite for SWNT nucleation, contrary to conventional experimental presumptions. The formation and coalescence of polyyne chains on the metal surface occur first, followed by the formation of the SWNT cap-precursor, "ring condensation", and the creation of an sp^2-hybridized carbon structure. In our simulations, the nucleation process takes approximately 400 ps. This first step occurs over a much longer time scale than the second stage of SWNT condensation (approximately 50 ps). We therefore observe SWNT nucleation to be akin to the rate-limiting step of the SWNT formation process.

In addition to the QM/MD simulation of various stages of SWNT nucleation, growth, and healing processes, we have determined the effects of temperature, catalyst composition, and catalyst size on the kinetics and mechanism of SWNT growth. With respect to temperature dependence, we observe a "sweet-spot" with respect to the efficiency of SWNT growth. In addition, Ni-catalyzed SWNT growth is observed to be 70−100% faster compared to Fe-catalyzed SWNT growth, depending on the catalyst particle size. We also observe a noticeable increase in SWNT growth rates using smaller catalyst particles.

Finally, we review our recent QM/MD investigation of SWNT healing. In particular, we recount mechanisms by which adatom defects, monovacancy defects, and a "5-7 defect" are removed from a nascent SWNT. The effectiveness of these healing mechanisms depends on the rate at which carbon moieties are incorporated into the growing SWNT. Explicitly, we observe that healing is promoted using a slower carbon supply rate. From this rudimentary control of SWNT healing, we propose a route towards chirality-controlled SWNT growth.

Published on the Web 07/27/2010 www.pubs.acs.org/acr
10.1021/ar100064g © 2010 American Chemical Society

Introduction

The initial discovery of C_{60} buckminsterfullerene[1] and the subsequent observation of carbon nanotubes[2−4] by electron microscopy heralded a new era in molecular science and technology. These nanostructures (and in particular single-walled carbon nanotubes (SWNTs)) have since become the cornerstones of a number of bourgeoning academic and industrial fields due to their remarkable properties. Consequently, a great deal of literature concerning experimental and theoretical investigations of synthesis of SWNTs is available today (see refs 5 and 6, respectively, and references therein).

In this Account, we will detail our own recent investigations[7−15] of transition-metal-catalyzed nucleation, growth, and healing mechanisms of SWNTs using quantum mechanical molecular dynamical (QM/MD) methods. We have employed the self-consistent-charge density-functional tight-binding-based molecular dynamics (SCC-DFTB/MD) approach,[16,17] in conjunction with a finite electronic-temperature[18−20] in all of these simulations.

The vapor−liquid−solid (VLS) mechanism of SWNT growth[21,22] suggests that SWNT synthesis begins with co-condensation of carbon and metal atoms from vapor, forming a liquid metal carbide phase. When supersaturation is ultimately reached, the solid phase nanotubes begin to grow. This thesis was derived from a range of experimental and theoretical data. SWNT condensation itself is initiated by the formation/nucleation of a carbon "cap" precursor on the catalyst nanoparticle surface. Following this nucleation, "cap-to-tube" transformation then takes place, during which a nanotube sidewall is constructed between the catalyst particle and the nucleated cap precursor. Finally, continued growth of the SWNT structure becomes dominant, in which the nanotube sidewalls are elongated by the continued incorporation of carbon from the surrounding medium. The following three sections of this Account are organized according to these corresponding individual stages in the SWNT nucleation and growth mechanism. Following these discussions, we will describe our recent investigations of the dependence of SWNT growth on several pertinent environmental factors, including catalyst composition, catalyst size, and growth temperature. We will then discuss the phenomena of SWNT healing and chirality-controlled SWNT growth, and their dependences on the rate at which carbon is incorporated into the nanotube during the growth process. Finally, we will place the results of our QM/MD simulations in an experimental context and provide an outlook of future QM/MD investigations into SWNT growth phenomena.

Fe_{38}-Catalyzed SWNT Nucleation

We have previously investigated SWNT nucleation using QM/MD methods.[11] Initially, 30 C_2 moieties were supplied to an equilibrated Fe_{38} nanoparticle at 1500 K during 30 ps. The resultant Fe−C complex was then annealed for a further 410 ps. The use of C_2 as a carbon precursor here is justified, since its abundance was found to be directly correlated to the nucleation process.[23]

The evolution of a single SWNT cap nucleation QM/MD trajectory is shown in Figure 1 and the accompanying movie M1. SWNT nucleation was composed of three distinct periods. Initially, C_2 units, once bound to the metal surface, diffused, occasionally fused, and formed longer polyyne chains. This stage was the rate-limiting step of the nucleation process, requiring more than 100 ps (see Figure 1b). During this period, these polyyne chains preferentially exhibited Fe−C_n−Fe type arrangements, with the catalyst surface progressively disintegrating due to the increasing C−Fe interaction. After this time, ring condensation was observed (Figure 1b), with 5- and 6-membered rings being formed preferentially. The first ring to condense on the catalyst surface was a 5-membered ring; this was observed to be a general trend in all trajectories computed (10 in total). This pentagon-first pattern is consistent with our previous observations of metal-catalyst-free fullerene nucleation.[24] The formation of the first carbon pentagon generally occurred via a sequence that included three distinct stages and is depicted in Figure 1c. In step (i), two polyyne chains fused, forming a Y-structure. The lone sp^2 carbon at the junction between these two branches served as a "cornerstone" for subsequent cyclization of the two branches. The two branches of the Y subsequently diffused over the catalyst surface toward each other. With respect to the original cornerstone carbon atom, the optimal distance for bond formation between the respective carbon atoms of each branch corresponded to the position of the atoms second from the cornerstone. There was therefore a greater possibility of bond formation between these two carbons, thus leading to the preferential formation of 5-membered rings (step (ii)). The observed longevity of 5-membered rings here was a result of the stability that these structures possess on the highly convex catalyst surface, imposed by the relatively small diameter of the catalyst nanoparticle.[25] The initial 5-membered ring then acted as an anchor for subsequent ring condensation that ultimately led to the nucleation of a SWNT cap structure on the catalyst surface. During this condensation stage, 5- or 6-membered rings

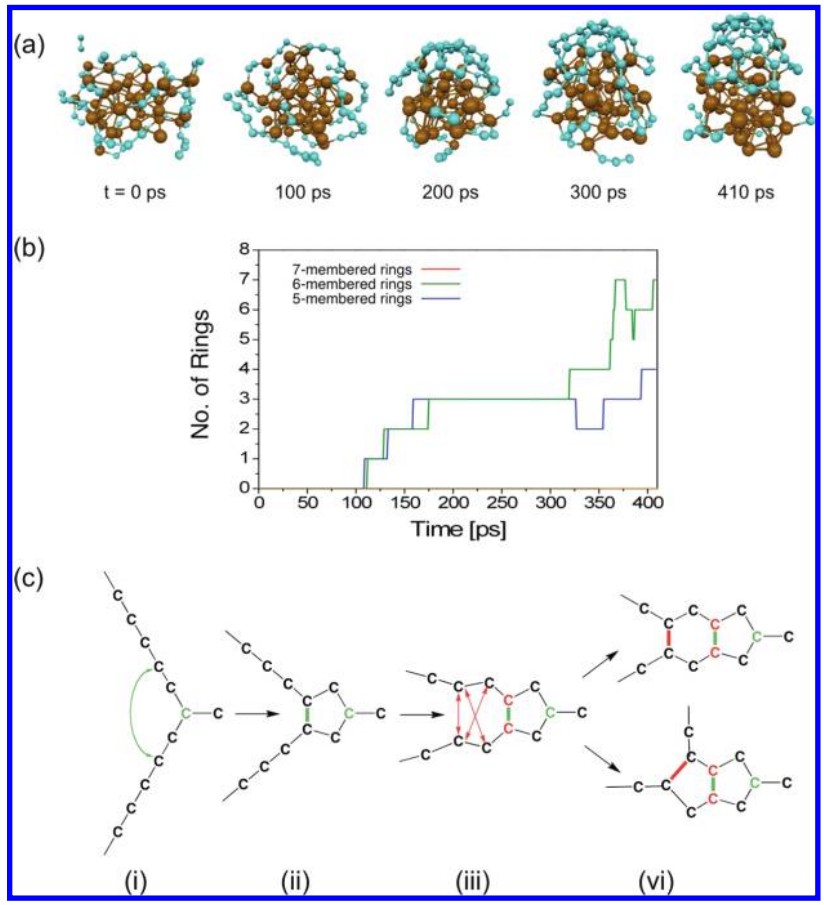

FIGURE 1. (a) SWNT nucleation on Fe_{38} at 1500 K, (b) corresponding ring addition, and (c) observed SWNT nucleation mechanism. Cyan and brown spheres represent carbon and iron atoms, respectively.

were formed with no discernible preference, due to the existence of a C−C moiety (instead of a single atom) as the cornerstone of the new Y-structure.

It is noted here that polycyclic carbon clusters observed during SWNT nucleation retained branched polyyne chains throughout our simulations. This observation parallels that made with respect to fullerene cage self-assembly.[24] It is concluded therefore that these chains are essential for both extension of the sp^2-hybridized carbon network (via ring condensation, described above) and anchoring of the nucleating cap fragment to the catalyst surface. Despite the observed similarities between SWNT and fullerene nucleation, it is clear that the catalyst nanoparticle plays a crucial role during the former process. In particular, the catalyst localizes the decomposed carbon precursor species, impedes polyyne diffusion (and hence ring condensation), and, perhaps most importantly, prevents the open end of the nucleating cap structure from closing. The latter role was already postulated by Smalley and co-workers in 1996.[26]

Fe_{38}-Catalyzed "Cap-to-Tube" Transformation

We have previously investigated the second stage of the SWNT formation process, namely, the cap-to-tube transformation, on a number of occasions.[10,12,14,15] In particular, we have demonstrated this phenomenon using both C_{40} and C_{20} cap precursors on Fe_{38} nanoparticles (the existence of both precursors being assumed a priori). These two transformations are shown in Figures 2 and 3, respectively. The latter cap-to-tube transformation is also illustrated in the accompanying movie M2.

In the case of cap-to-tube transformation using a C_{40} cap-precursor,[10] the transformation was induced at 1500 K by the supply of 40 gas-phase carbon atoms in 20 ps to the catalyst surface of an annealed C_{40}-Fe_{38} model system. The structure was then annealed for a further 140 ps. The sp^2-hybridized carbon network of the cap precursor was extended by the addition of 5- and 6-membered rings at the cap-catalyst boundary (Figure 2a). Ultimately, the ratio of these newly formed polygonal rings was ca. 1:1. In this case, no 7-mem-

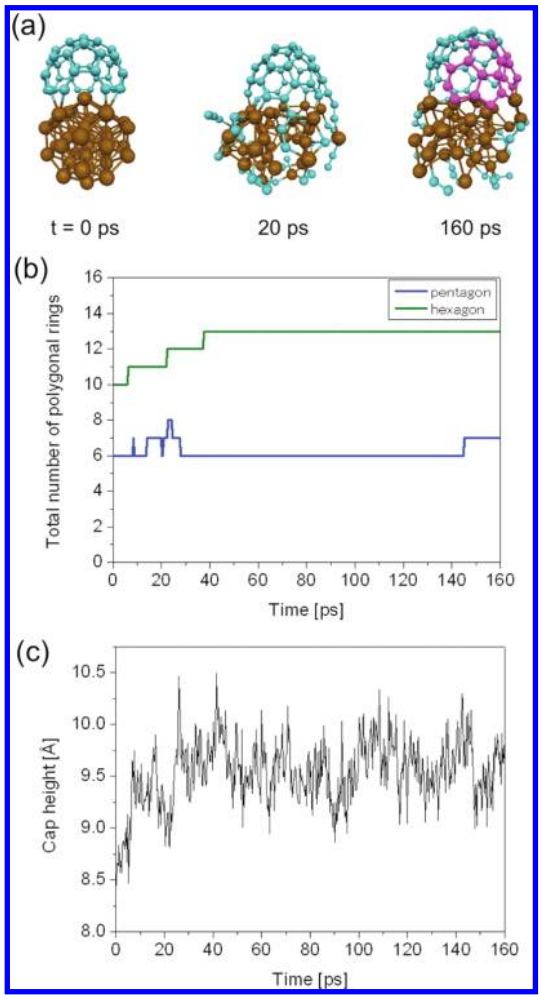

FIGURE 2. (a) Fe_{38}-catalyzed cap-to-tube transformation using C_{40} at 1500 K, (b) corresponding ring addition, and (c) corresponding cap height. Color conventions as in Figure 1; pink spheres represent carbons in newly formed polygonal rings.

bered rings were added to the cap precursor (Figure 2 b). One of the roles of the catalyst during CVD SWNT growth, namely the mediation/impedance of carbon addition into the nanotube at its base during growth, is illustrated succinctly in Figure 2. This is somewhat counterintuitive to the traditional definition of a chemical catalyst (i.e., a species employed to enhance the kinetics of a particular reaction). Also evident from Figure 2 is the fact that the newly added polygonal rings in the cap precursor were approximately coincident with the spatial axis of growth itself. This is therefore a demonstration of nanotube sidewall construction, and hence cap-to-tube transformation, during the earliest stages of metal-catalyzed SWNT growth.

A more dramatic example of the cap-to-tube transformation phenomenon was observed using a C_{20} cap precursor,[12] and this is depicted in Figure 3. In this case, 66 gas-phase carbon atoms were supplied at a constant rate to randomly chosen carbon atoms in the cap fragment during 40 ps at 1500 K. From Figure 3, it is evident that cap-to-tube transformation in this case took place quickly (within 40 ps), compared to the transformation observed using a C_{40} cap. Once again, the newly formed polygonal rings in the cap precursor were added along the axis of growth, thereby demonstrating the progressive construction of the nanotube sidewall. However, this was achieved by a contrasting mechanism from that discussed previously, as one might anticipate. Comparison of Figures 2b and 3b illustrates this contrast. The high number of 5- and 7-membered rings (and also 3- and 4-membered rings, although not shown in Figure 3b) was a consequence of the direct addition of carbon to the established sp^2-network, and the subsequent accommodation of the newly added carbon via the rearrangement of the sp^2-hybridized cap structure. The dissociation or migration of C_2 or short polyyne units from the expanding sp^2-network was also frequently observed. On occasion, these moieties migrated toward the cap−catalyst region and were incorporated directly into the base of the evolving cap structure. Once in this position, these polyyne chains contributed to ring formation by either self-isomerization or interaction with adjacent polyyne chains. Such polyyne dissociation−migration−isomerization phenomena were observed to increase in frequency as the cap-to-tube transformation proceeded.

Fe_{38}-Catalyzed Continued SWNT Growth

We have previously demonstrated[8] continued SWNT growth at 1500 K using QM/MD methods. This was achieved using a model system consisting of a SWNT fragment supported by an Fe_{38} nanoparticle (Figure 4a). Upon rapid supply of carbon atoms to randomly selected target atoms in the SWNT rim, growth (Figure 4b) occurred via the immediate insertion of the incident carbon atoms into the existing SWNT−catalyst boundary. Generally, short bridging structures featuring carbon or C_2 (comparable to the "wobbling" C_2 observed during the self-capping of open-ended SWNTs[27]) were observed between the SWNT and the Fe_{38} nanoparticle (Figure 4c). In step (i), an incident carbon atom approached the existing SWNT−catalyst boundary. Subsequently, this carbon atom formed a trigonal C−C−Fe intermediate species (step (ii)) by insertion into an existing C−Fe bond. This intermediate species, due to its inherently high ring torsion, was very short-lived and ultimately became a C−C−Fe bridging structure between the catalyst and the SWNT (step (iii)). The formation of these carbonaceous bridging structures generally preceded the formation of 5-, 6-, 7-, and occasionally 8-membered rings at the SWNT base. Nevertheless, the presence of long polyyne

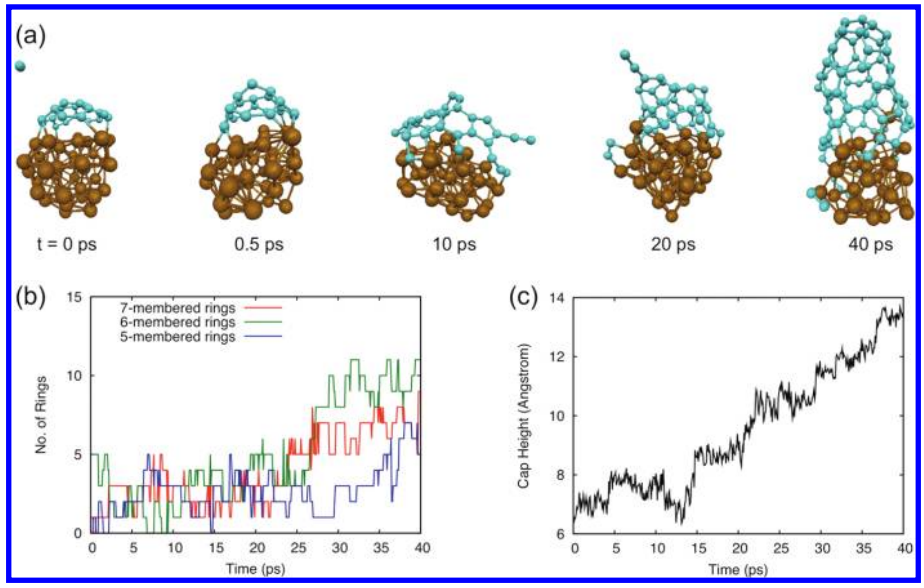

FIGURE 3. (a) Fe_{38}-catalyzed cap-to-tube transformation using C_{20} at 1500 K, (b) corresponding ring addition, and (c) corresponding cap height. Color conventions as in Figure 1.

chains (i.e., $n \geq 4$) was not a prerequisite for continued SWNT growth on Fe_{38}, as shown schematically in Figure 4d. The short bridging structure, formed by the incorporation of an incident carbon atom into the SWNT−catalyst boundary, remained in the complex for some time (steps (i), (ii)). During this time, frequent bond breaking/formation between constituent carbon and iron atoms was observed. In step (iii), the terminal carbon atoms of adjacent bridging structures ultimately formed a bond and thus a 6-membered ring. Due to the stability of this ring structure, it was effectively a permanent feature of the SWNT from this point on. Formation of a 5-membered ring (Figure 4e) occurred by a similar process, in that the ring structure was the result of the interaction of adjacent bridging structures at the base of the SWNT. In this case, however, the carbon atom involved in the ring closure process was not terminal (step (iii)). The 5-membered ring thus formed, shown in step (iv), was also very stable and persisted in the SWNT structure.

Dependence of SWNT Growth on Catalyst Composition, Size, and Reaction Temperature

We have recently compared SWNT growth mechanisms and rates as a function of both catalyst size and composition.[13,14] This comparison is outlined in Table 1. In this case, SWNT growth was modeled using C_{40}−M_x (M = Fe, Ni; x = 38, 55) complexes and induced by supplying gas-phase carbon atoms to the SWNT−catalyst boundary at 1500 K. From Table 1, it is evident that the rate of SWNT growth increased dramatically by using a nickel catalyst, instead of an iron catalyst. Explicitly, these increases were ca. 69% (M_{55}) and 106% (M_{38}) following 50 ps of growth simulation. This increase in SWNT growth rate upon using nickel catalysts correlated with a noticeably different SWNT growth mechanism from that observed using iron catalysts, defined by the presence and persistence of long C_n ($n \geq 3$) chains located between the C_{40} cap and the nickel catalyst particle. Ring formation in this case was driven by the simultaneous extension and contraction (via self-isomerization) of these polyyne chains at the SWNT base.[13] Conversely, the polyyne chains observed in Fe-catalyzed growth were generally shorter (primarily C_2 and C_3 units) and existed for shorter periods of time. The observed difference between the two metal catalysts can be attributed to the stronger carbon−catalyst adhesion energy observed for iron, compared to that observed for nickel.[14]

With respect to the role of catalyst size on the mechanism and rate of SWNT growth, data in Table 1 indicate that an increase in catalyst size corresponds to a decrease in the SWNT growth rate. This trend was independent of the elemental composition of the catalyst particle. For example, Ni_{38}-catalyzed SWNT growth was ca. 50% faster than Ni_{55}-catalyzed SWNT growth, whereas this ratio was 23% for the case of Fe-catalyzed SWNT growth. Nevertheless, the SWNT growth mechanism was independent of the catalyst particle size. These differences in M_x-catalyzed SWNT growth rates (x = 38, 55) were attributed primarily to the increases in catalyst particle surface area and volume. Essentially, a larger catalyst particle provided a greater domain over/through which carbon could diffuse, before contributing to SWNT growth.

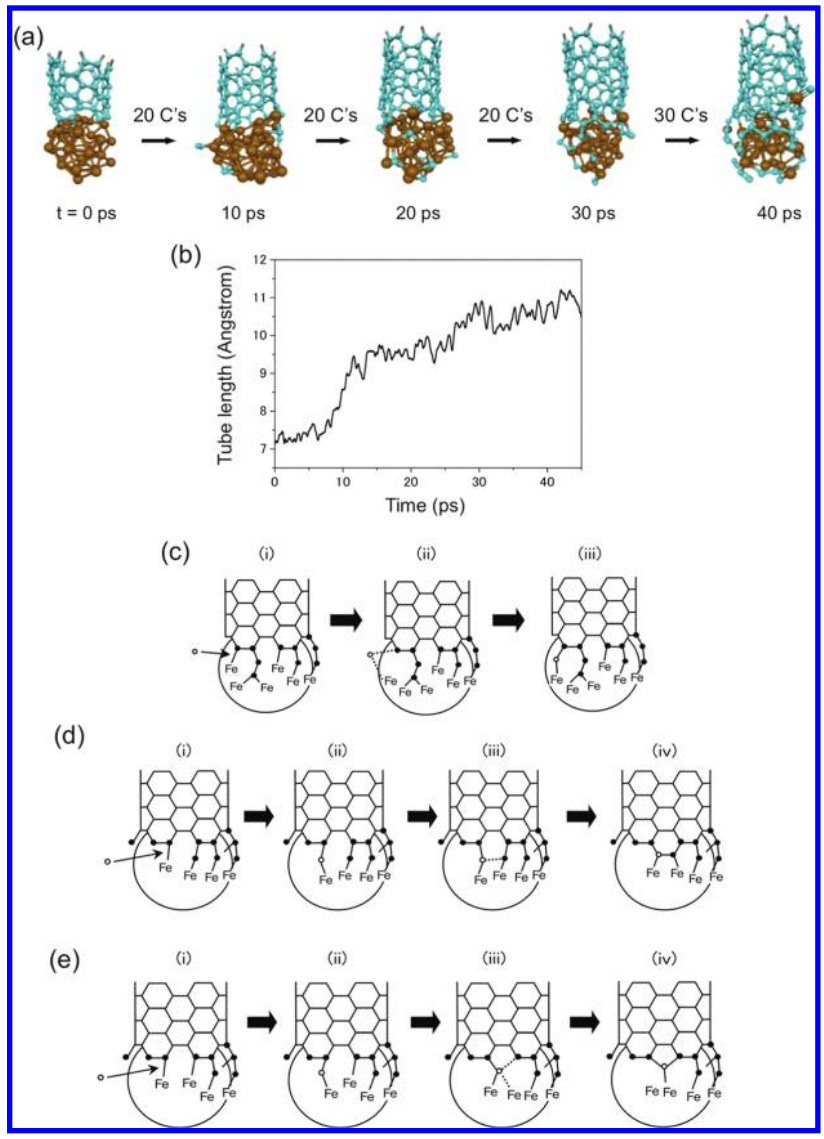

FIGURE 4. (a) Continued growth of a SWNT fragment on Fe_{38} at 1500 K, (b) corresponding SWNT height, and mechanisms of (c) carbon atom incorporation into C−Fe boundary, (d) 6-membered ring addition, and (e) 5-membered ring addition. Color conventions as in Figure 1; white spheres represent H atoms.

TABLE 1. Dependence of C_{40} Cap Growth on Catalyst Size and Composition: Average Growth Rate and Number of Added Carbons and Polygonal Rings after 50 ps of Simulation Using Fe_{38}, Fe_{55}, Ni_{38}, and Ni_{55} Catalysts (All Data Averaged over 10 Trajectories)

			number of *n*-membered rings added to SWNT		
catalyst	growth rate ($\times 10^{-2}$ Å ps^{-1})	number of carbons added to SWNT	$n = 5$	$n = 6$	$n = 7$
Fe_{55}	2.879	51.0	6.2	6.5	4.4
Fe_{38}	3.542	55.2	6.2	9.2	4.3
Ni_{55}	4.874	62.4	9.0	9.0	5.9
Ni_{38}	7.299	64.8	9.2	10.2	6.5

This phenomenon is shown in Figure 5a, from which an inversely proportional relationship between SWNT growth rate and the amount of "free carbon" present (i.e., those carbon atoms that are not located in the sp^2-hybridized nanotube structure) is evident. An inverse relationship between SWNT growth rate and the instantaneous mobility of these free carbon atoms is also evident in Figure 5b. The instantaneous mobility at the *i*th MD step is defined here as the total distance traveled by *all* free carbon atoms (with respect to the catalyst particle center of mass) between the $(i - 1)$th and *i*th MD steps.

The temperature dependence of SWNT growth simulated using a (5,5) SWNT-Fe_{38} model complex is outlined in Table 2. It is evident from this table that SWNT growth was optimal at 1500 K. For example, the SWNT growth rate at this temperature was ca. 46% and 23% larger than those observed at 1000 and 2000 K, respectively. It is concluded from Table 2 that the rate of SWNT growth depended on a number of factors, such as the ratios of 5-, 6-, and 7-membered rings added

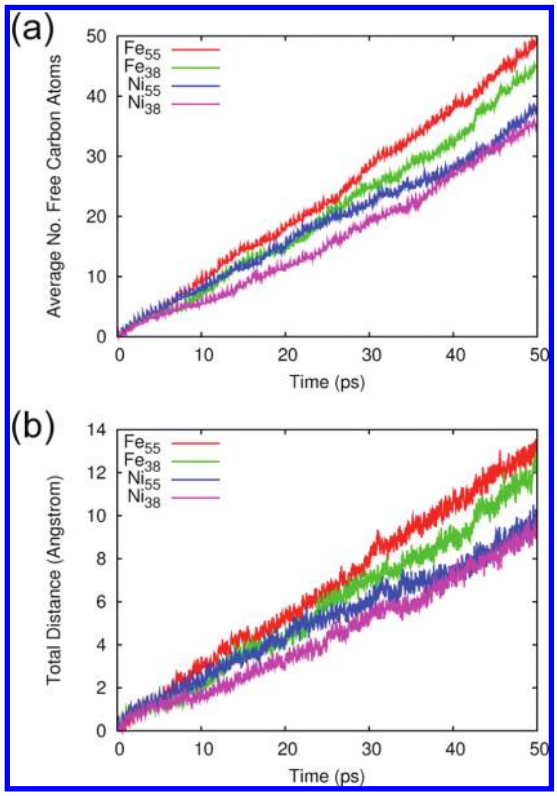

FIGURE 5. (a) Average number of free carbon atoms and (b) average free carbon instantaneous mobility observed in M_x-catalyzed SWNT growth after 50 ps simulation (M = Fe, Ni; x = 38, 55).

TABLE 2. Temperature Dependence of Fe_{38}-Catalyzed (5,5)-SWNT Growth: Average Growth Rate and Number of Added Carbons and Polygonal Rings after 45 ps of Simulation (Data Averaged over 10 Trajectories)

			number of *n*-membered rings added to SWNT		
T (K)	growth rate ($\times 10^{-2}$ Å ps^{-1})	number of carbons added to SWNT	$n = 5$	$n = 6$	$n = 7$
1000	3.48	52.9	4.7	2.5	4.8
1500	5.07	50.1	5.7	1.9	5.2
2000	4.13	42.7	5.7	1.7	5.3

to the growth of the nanotube sidewall. Although the number of 5- and 7-membered rings added to the SWNT increased with temperature, the number of 6-membered rings added in fact decreased. As noted above, the propensity toward 5- and 7-membered ring formation arose from the addition of carbon atoms directly into the base of the SWNT structure. Thus, 5- and 7-membered ring formation was more favorable at higher temperatures, due to the increase in the kinetic energy (and hence velocity) of the SWNT carbon atoms.

SWNT Healing and Chirality-Controlled Growth

Recently, we have elucidated the dependence of SWNT healing (i.e., the removal of defects from the sp^2 network) on the

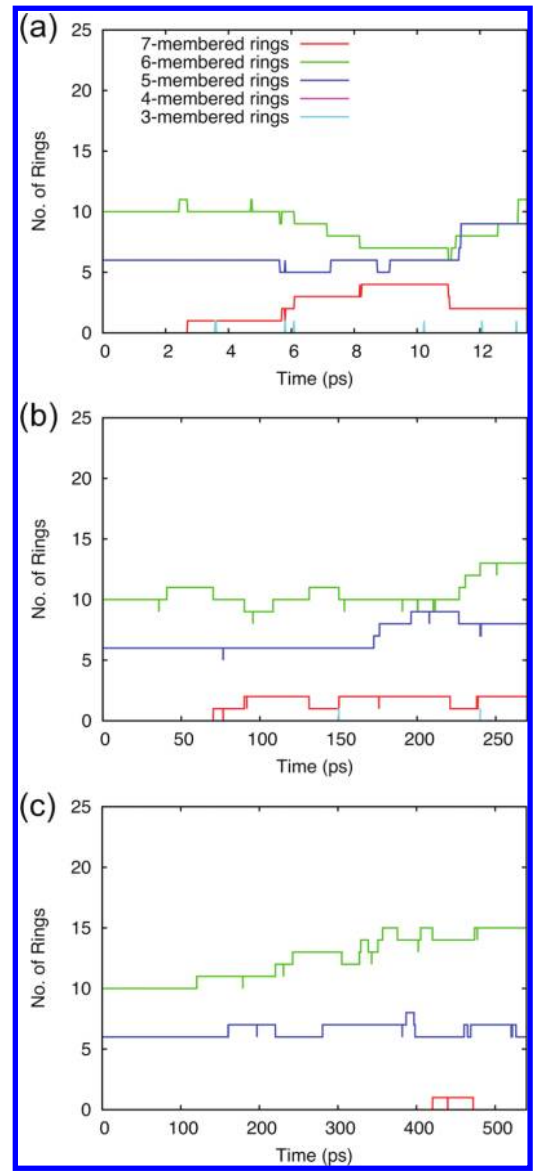

FIGURE 6. Dependence of SWNT healing on carbon supply rate: comparison of SWNT ring additions (27 carbon atoms added) using carbon supply rates of 1 C/(a) 0.5 ps, (b) 10 ps, and (c) 20 ps.

rate of carbon supply.[15] The latter is effectively an approximation to the carbon precursor decomposition rate. Using three rates of carbon atom supply to the C−Fe boundary, namely, 1 C/0.5, 10.0, and 20.0 ps (rates denoted using "fast", "slow", and "very slow", respectively), SWNT growth was induced in a C_{40}−Fe_{38} complex at 1500 K. The dynamics of cap growth using slow and very slow supply differed substantially, in both quantitative and qualitative senses, from those using fast supply (see Figure 6). Most notably, a greater, more orderly extension of the original C_{40} cap structure was attained using slow and very slow supply simulations. For example, Figure 6 shows the ring counting statistics of individual C_{40}−Fe_{38} growth trajectories following the addition of 27 carbon atoms during periods of 13.5 (fast), 270 (slow), and 540

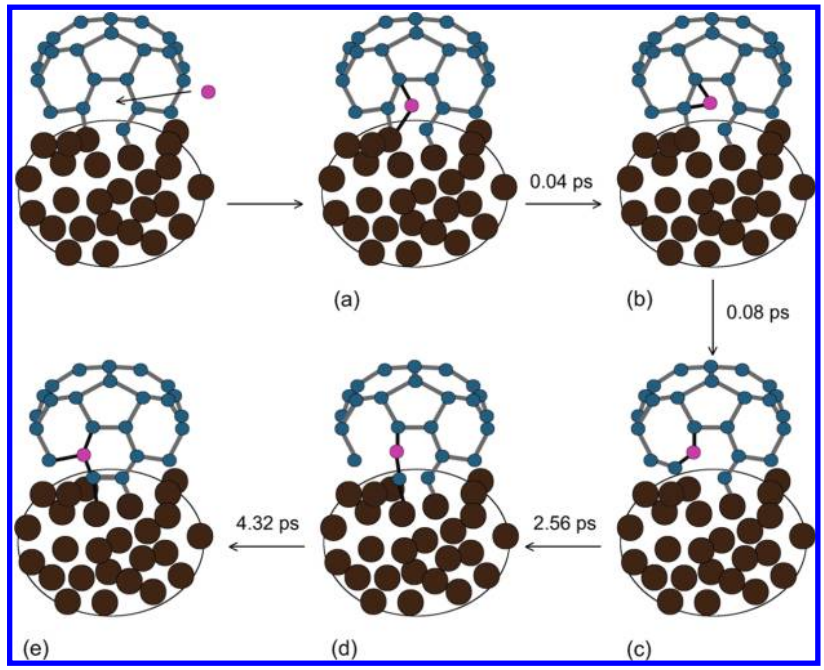

FIGURE 7. Healing during SWNT growth: a schematic depiction of 5-7 defect removal from a carbon cap structure via ring isomerization at 1500 K. Color conventions as in Figure 1; the pink sphere represents the incident carbon atom (see text). Only relevant bonds are shown; new bonds formed during the isomerization are black.

(very slow) ps. It is immediate from this figure that the frequencies at which 5- and 7-membered rings were formed dramatically decreased using slow and very slow carbon supply rates. Most notably, following 540 ps of very slow supply SWNT growth simulation, the net additions of 5- or 7-membered rings to the C_{40} cap were zero. This is in effect a demonstration of chirality-controlled SWNT growth, since growth was driven exclusively by the addition of 6-membered rings. The addition of 6-membered rings to the C_{40} cap was also promoted substantially using slow and very slow supply. The net effect of fast carbon atom supply was, in fact, the opposite, namely, the removal of 6-membered rings via the formation of 7-membered rings as discussed above. These trends were concomitant with a decrease in the number of "free" C/C_n units bound to the catalyst surface (i.e., those that were not contributing to the growth process), and attributed to the decreased rate of carbon atom supply itself. In essence, the slower supply rate provided an increased amount of time during which the supplied carbon atom was free to diffuse of the catalyst surface relatively unheeded, ultimately migrating to the SWNT−catalyst boundary. The relationship between the carbon atom supply rate and the consequent SWNT growth rate was also established. Following the addition of 27 carbons to the C_{40} cap structure using fast, slow, and very slow supply, the "cap heights" corresponding to Figure 6a, b, and c were 0.389, 1.587, and 2.203 Å, respectively. It is concluded therefore that a lower rate of carbon supply promotes both the "efficiencies" of SWNT growth and healing.

Mechanisms by which adatoms, monovacancy, and 5-/7-membered ring defects (denoted as 5-7 defects) are removed from the C_{40} cap during growth have also recently been observed in our QM/MD simulations of SWNT growth.[15] The latter mechanism featured a ring isomerization akin to a Stones−Wales transformation, and it is depicted schematically in Figure 7 and the accompanying movie M3. The 5-7 defect was removed in five distinct steps. First, in step (a), an incident carbon atom formed a briefly lived adatom defect at the SWNT−catalyst boundary. Following a fleeting, 3-membered ring intermediate structure (step (b)), insertion of this incident carbon atom was observed, forming a 7-membered ring (step (c)). This 7-membered ring was relatively stable and existed for a further 2.48 ps. It is noted here that the adjoining 5-membered ring was held open throughout the entire isomerization process by the surface iron atoms in the catalyst nanoparticle. Following 2.48 ps, the C−C bond adjacent to the catalyst surface was cleaved, and the neighboring C−C bond rotated about an approximate angle of 45°. This open-ring structure (step (d)) was quite stable, existing for a further 1.76 ps, after which two 6-membered rings were formed, replacing the original 5-7 defect.

From consideration of the time scale over which this healing mechanism occurs (and those over which adatom and

monovacancies healing mechanisms occur, ca. 1−25 ps), it is evident that the rate of SWNT healing is determined by the relative rates of defect addition to and removal from the SWNT structure. Decreasing the carbon precursor decomposition rate will therefore ultimately result in the presence of fewer defects in the nanotube sidewall. We propose that such a rudimentary control during SWNT growth is essential for chirality-controlled SWNT growth. Admittedly, these investigations of SWNT healing shed no light on the *origin* of the (*n*,*m*) chirality of the SWNT itself. Rather, they only indicate how chirality, once attained in the nascent SWNT cap, may be conserved during continued growth of the SWNT.

Comparison of QM/MD and Experimental Mechanisms of SWNT Nucleation and Growth

QM/MD methods provide a convenient, tractable medium by which atomistic details of physicochemical phenomena may be observed. The processes of SWNT nucleation and growth are no exception. In this work, we have reviewed our recent research that has shed light on the phenomena underpinning the nucleation and growth of SWNTs from a variety of transition-metal catalyst particles, at spatial and temporal scales beyond the reach of current experimental technology. We observe both consistencies and disparities between QM/MD predictions and experimental observations. For example, QM/MD simulations have successfully modeled the individual stages of the SWNT nucleation and growth and have elucidated the mechanism of SWNT healing, as has been demonstrated in this Account. Nevertheless, SWNT growth rates observed in our QM/MD simulations are several orders of magnitude larger than those typical of in situ growth rates.[28−35] A direct comparison between these data is relatively futile, however, due to the simplistic model system employed in our QM/MD simulations of SWNT growth. A variety of pertinent factors, such as environmental pressure, the presence of catalyst substrate, and so on, are neglected in our models. The rates at which carbon is added to the growing SWNT structure (i.e., the rate of feedstock decomposition) in these simulations also exceed those reported experimentally. The sheer number of differing experimental synthesis techniques, and consequent SWNT growth rates, reported in the literature (see refs 5 and 14, and references therein) makes such a comparison even more futile. It is more reasonable instead to compare the relative trends observed in our QM/MD simulations with those observed experimentally. For instance, we have observed that Ni-catalyzed SWNT growth proceeds at a greater rate than does Fe-catalyzed SWNT growth. This trend is consistent with the presumption of Mora and Haratyunyan,[36] one that was based upon the relative abilities of nickel and iron nanoparticles to catalytically decompose CH_4 feedstock observed experimentally.

Perhaps the most significant impasse between present theoretical and experimental models of SWNT nucleation/growth concerns the existence of a stable metal-carbide particle prior to SWNT nucleation. As discussed in this work, our QM/MD simulations indicate that such a particle is not required for the nucleation of a SWNT to take place. Similarly, recent tight-binding Monte Carlo[37] and DFT[38] studies suggest that a regular crystalline metal-carbide structure is unstable under low pressure conditions. These findings suggest that, depending on the environmental pressure, the carbon within the metal-carbide particle naturally migrates to the "subsurface" layers of the catalyst particle instead. Nevertheless, regular crystalline structures, such as Fe_3C[39,40] and Ni_3C,[41] have been observed during SWNT nucleation and growth, by both transmission electron microscopy and electron diffraction techniques. Whether these metal-carbide phases are a necessary prerequisite for SWNT nucleation and growth, or coincidentally develop under the growth conditions has not yet been fully established.

Conclusions and Outlook

In this Account, we have reviewed our recent QM/MD investigations of SWNT nucleation, growth, and healing. These theoretical findings are qualitatively consistent with a SWNT nucleation and growth mechanism that has been extensively supported by experimental data. Our simulations consistently demonstrate a self-organization mechanism that consists of random growth followed by defect healing. Similarly, the dependence of SWNT growth on several pertinent environmental factors, including temperature, catalyst composition, and catalyst size, has also been established using QM/MD techniques. In this respect, our QM/MD investigations have pre-empted experimental determination of the effects of catalyst composition and size on the mechanism and nature of SWNT growth. However, by no means do we acquiesce and claim that QM/MD simulations of SWNT can shed no new light on SWNT growth phenomena. There are many points over which current experimental and theoretical models fail to agree. Most notably in this respect is the question as to whether a metal-carbide species is a necessary precursor for SWNT nucleation. In addition, there are many other aspects of SWNT growth that are amenable to further theoretical study, such as the origin of (*n*,*m*) SWNT chirality, the demonstration of chirality-controlled growth over extended time scales, and

mechanisms of SWNT nucleation and growth on non-transition-metal catalysts.

Financial support from a Core Research for Evolutional Science and Technology (CREST) grant courtesy of the Japanese Science and Technology Agency (JST), and the Special Coordination Funds for Promoting Science and Technology (SCF) commissioned by the Ministry of Education, Culture, Sports, Science and Technology (MEXT) of Japan is greatly appreciated. Computational support from the Research Center for Computational Science (RCCS), Okazaki Research Facilities, National Institutes for Natural Sciences and the Academic Center for Computing and Media Studies (ACCMS) at Kyoto University are also acknowledged.

BIOGRAPHICAL INFORMATION

Alister Page was born in Newcastle, Australia. He received undergraduate degrees in mathematics and chemistry at The University of Newcastle, Australia, graduating in 2005. He obtained his Ph.D. (2008) at The University of Newcastle, Australia, for ab initio studies of rovibrational spectroscopy under the supervision of Prof. Ellak I. von Nagy-Felsobuki. He is currently a postdoctoral fellow at the Fukui Institute for Fundamental Chemistry (FIFC), Kyoto University, investigating nanoscale self-assembly phenomena using QM/MD methods.

Yasuhito Ohta was born in Ishikawa, Japan. He received both undergraduate and doctoral educations at Kanazawa University, before taking on postdoctoral positions at Pennsylvania State University (Prof. Hammes-Schiffer) and Kyoto University (Prof. Morokuma). In 2009, he was appointed Associate Professor in the Department of Chemistry of Nara Women's University, Japan. His current research interests include molecular self-assembly of nanostructures, nuclear quantum effects in condensed phases, quantum control of chemical reactions, and molecular dynamics in intense laser fields.

Stephan Irle obtained his diploma in chemistry at the University of Siegen in Germany and a Ph.D. from the University of Vienna in Austria. Starting from 1997, he has worked with Prof. Keiji Morokuma and subscribers of the Emerson Center at Emory University on many problems in theoretical and computational chemistry. He has coordinated the computational nanomaterials research efforts of the Morokuma group and increasingly used quantum chemical molecular dynamics simulations in the study of nanomaterial self-assembly processes far from thermodynamic equilibrium. After a brief stay at the Fukui Institute for Fundamental Chemistry at Kyoto University in 2006, he has been appointed as Associate Professor at the Institute for Advanced Research and Department of Chemistry at Nagoya University where he continues theoretical studies on nanomaterials and dynamic processes of complex reaction systems under extreme conditions.

Keiji Morokuma is Research Leader at the Fukui Institute for Fundamental Chemistry at Kyoto University, and Professor Emeritus at Emory University. Having obtained his academic degrees from Kyoto University, he was a professor at the University of Rochester and Institute for Molecular Science in Okazaki, Japan, and William H. Emerson Professor of Chemistry and Director of the Cherry L. Emerson Center for Scientific Computation at Emory University before taking up his present appointment. Prof. Morokuma has authored over 670 scientific publications and has received scientific awards including the Imperial Prize and Japan Academy Prize, the Japan Chemical Society Award, Schrödinger Medal from World Association of Theoretical Organic Chemists, and Fukui Medal of Asian Pacific Association of Theoretical & Computational Chemists. He was the President of the International Academy of Quantum Molecular Science from 2000 to 2006.

FOOTNOTES

* To whom all correspondence should be addressed. E-mail: sirle@iar.nagoya-u.ac.jp (S.I.); morokuma@fukui.kyoto-u.ac.jp.

REFERENCES

1 Kroto, H. W.; Heath, J. R.; O'Brien, S. C.; Curl, R. F.; Smalley, R. E. C_{60}: Buckminsterfullerene. *Nature* **1985**, *318*, 162–163.

2 Iijima, S. Helical Microtubules of Graphitic Carbon. *Nature* **1991**, *354*, 56–58.

3 Iijima, S.; Ichihashi, T. Single-Shell Carbon Nanotubes of 1-nm Diameter. *Nature* **1993**, *363*, 603–605.

4 Bethune, D. S.; Klang, C. H.; de Vries, M. S.; Gorman, G.; Savoy, R.; Vazquez, J.; Beyers, R. Cobalt-catalysed growth of carbon nanotubes with single-atomic-layer walls. *Nature* **1993**, *363*, 605–607.

5 Awasthi, K.; Srivsatava, A.; Srivastava, O. N. Synthesis of Carbon Nanotubes. *J. Nanosci. Nanotechnol.* **2005**, *10*, 1616–1636.

6 Irle, S.; Ohta, Y.; Okamoto, Y.; Page, A.; Wang, Y.; Morokuma, K. Milestones in molecular dynamics simulations of single-walled carbon nanotube formation: A brief critical review. *Nano Res.* **2009**, *2*, 755–767.

7 Irle, S.; Okamoto, Y.; Ohta, Y.; Zheng, G.; Morokuma, K. In *DFT Calculations on Fullerenes and Carbon Nanotubes*; Basiuk, V. A., Irle, S., Eds.; Research Signpost: Trivandrum, India, 2008.

8 Ohta, Y.; Okamoto, Y.; Irle, S.; Morokuma, K. Rapid Growth of a Single-Walled Carbon Nanotube on an Iron Cluster: Density-Functional Tight-Binding Molecular Dynamics Simulations. *ACS Nano* **2008**, *2*, 1437–1444.

9 Ohta, Y.; Okamoto, Y.; Irle, S.; Morokuma, K. Temperature Dependence of Iron-Catalyzed Continued Single-Walled Carbon Nanotube Growth Rates: Density Functional Tight-Binding Molecular Dynamics Simulations. *J. Phys. Chem. C* **2009**, *113*, 159–169.

10 Ohta, Y.; Okamoto, Y.; Irle, S.; Morokuma, K. Density-Functional Tight-Binding Molecular Dynamics Simulations of SWCNT Growth by Surface Carbon Diffusion on an Iron Cluster. *Carbon* **2009**, *47*, 1270–1275.

11 Ohta, Y.; Okamoto, Y.; Page, A. J.; Irle, S.; Morokuma, K. Quantum Chemical Molecular Dynamics Simulation of Single-Walled Carbon Nanotube Cap Nucleation on an Iron Particle. *ACS Nano* **2009**, *3*, 3413–3420.

12 Ohta, Y.; Okamoto, Y.; Irle, S.; Morokuma, K. Single-Walled Carbon Nanotube Growth from a Cap Fragment on an Iron Nanoparticle: Density-Functional Tight-Binding Molecular Dynamics Simulations. *Phys. Rev. B* **2009**, *79*, 195415.

13 Page, A. J.; Irle, S.; Morokuma, K. Polyyne Chain Growth and Ring Collapse Drives Ni-Catalyzed SWNT Growth: A QM/MD Investigation. *J. Phys. Chem. C* **2010**, *114*, 8206–8211.

14 Page, A. J.; Minami, S.; Ohta, Y.; Irle, S.; Morokuma, K. Comparison of single-walled carbon nanotube growth from Fe and Ni nanoparticles using quantum chemical molecular dynamics methods. *Carbon* **2010**, *48*, 3014–3026.

15 Page, A. J.; Ohta, Y.; Okamoto, Y.; Irle, S.; Morokuma, K. Defect Healing during Single-Walled Carbon Nanotube Growth: A Density-Functional Tight-Binding Molecular Dynamics Investigation. *J. Phys. Chem. C* **2009**, *113*, 20198–20207.

16 Elstner, M.; Porezag, D.; Jungnickel, G.; Elsner, J.; Haugk, M.; Frauenheim, T.; Suhai, S.; Seifert, G. Self-Consistent-Charge Density-Functional Tight-Binding Method for Simulations of Complex Materials Properties. *Phys. Rev. B* **1998**, *58*, 7260–7268.

17 Zheng, G.; Witek, H. A.; Bobadova-Parvanova, P.; Irle, S.; Musaev, D. G.; Prabhakar, R.; Morokuma, K.; Lundberg, M.; Elstner, M.; Kohler, C.; Frauenheim, T. Parameter

Calibration of Transition-Metal Elements for the Spin-Polarized Self-Consistent-Charge Density-Functional Tight-Binding (DFTB) Method; Sc, Ti, Fe, Co, and Ni. *J. Chem. Theory Comput.* **2007**, *3*, 1349–1367.

18 Wagner, F.; Laloyaux, T.; Scheffler, M. Errors In Hellmann-Feynman Forces Due To Occupation-Number Broadening and How They Can Be Corrected. *Phys. Rev. B* **1998**, *57*, 2102–2107.

19 Weinert, M.; Davenport, J. W. Fractional Occupations and Density-Functional Energies and Forces. *Phys. Rev. B* **1992**, *45*, 13709–13712.

20 Wentzcovitch, R. M.; Martins, J. L.; Allen, P. B. Energy Versus Free-Energy Conservation in First-Principles Molecular Dynamics. *Phys. Rev. B* **1992**, *45*, 11372.

21 Gavillet, J.; Thibault, J.; Stephan, O.; Amara, H.; Loiseau, A.; Ch., B.; Gaspard, J.-P.; Ducastelle, F. Nucleation and Growth of SWNTs: The Role of Metallic Catalysts. *J. Nanosci. Nanotechnol.* **2004**, *4*, 346–359.

22 Harris, P. J. F. Solid State Growth Mechanisms for Carbon Nanotubes. *Carbon* **2007**, *45*, 229–239.

23 Motaung, D. E.; Moodley, M. K.; Manikandan, E.; Coville, N. J. In situ optical emission study on the role of C_2 in the synthesis of single-walled carbon nanotubes. *J. Appl. Phys.* **2010**, *107*, 044308/1–15.

24 Irle, S.; Zheng, G.; Wang, Z.; Morokuma, K. The C_{60} Formation Puzzle "Solved": QM/MD Simulations Reveal the Shrinking Hot Giant Road of the Dynamic Fullerene Self-Assembly Mechanism. *J. Phys. Chem. B* **2006**, *110*, 14531–14545.

25 Fan, X.; Buczko, R.; Puretzky, A. A.; Geohegan, D. B.; Howe, J. Y.; Pantelides, S. T.; Pennycook, S. J. Nucleation of Single-Walled Carbon Nanotubes. *Phys. Rev. Lett.* **2003**, *90*, 145501/1–145501/4.

26 Thess, A.; Lee, R.; Nikolaev, P.; Dai, H.; Petit, P.; Robert, J.; Xu, C.; Lee, Y. H.; Kim, S. G.; Rinzler, A. G.; Colbert, D. T.; Scuseria, G. E.; Tomanek, D.; Fischer, J. E.; Smalley, R. E. Crystalline Ropes of Metallic Carbon Nanotubes. *Science* **1996**, *273*, 483–487.

27 Zheng, G.; Irle, S.; Elstner, M.; Morokuma, K. Quantum Chemical Molecular Dynamics Model Study of Fullerene Formation from Open-Ended Carbon Nanotubes. *J. Phys. Chem. A* **2004**, *108*, 3182–3194.

28 Kim, K.-E.; Kim, K.-J.; Jung, W. S.; Bae, S. Y.; Park, J.; Choi, J.; Choo, J. Investigation on the Temperature-Dependent Growth Rate of Carbon Nanotubes using Chemical Vapor Deposition of Ferrocene and Acetylene. *Chem. Phys. Lett.* **2005**, *401*, 459.

29 Puretzky, A. A.; Geohegan, D. B.; Jesse, S.; Ivanov, I. N.; Eres, G. In Situ Measurements and Modeling of Carbon Nanotube Array Growth Kinetics During Chemical Vapor Deposition. *Appl. Phys. A: Mater. Sci. Process.* **2005**, *81*, 223.

30 Bonard, J.-M.; Croci, M.; Conus, F.; Stockli, T.; Chatelain, A. Watching Carbon Nanotubes Grow. *Appl. Phys. Lett.* **2002**, *81*, 2836.

31 Yao, Y.; Liu, R.; Zhang, J.; Jiao, L.; Liu, Z. Raman Spectral Measuring of the Growth Rate of Individual Single-Walled Carbon Nanotubes. *J. Phys. Chem. C* **2007**, *111*, 8407.

32 Futaba, D. N.; Hata, K.; Yamada, T.; Mizuno, K.; Yumura, M.; Iijima, S. Kinetics of Water-Assisted Single-Walled Carbon Nanotube Synthesis Revealed by a Time-Evolution Analysis. *Phys. Rev. Lett.* **2005**, *95*, 056104.

33 Xiang, R.; Einarsson, E.; Okawa, J.; Miyauchi, Y.; Maruyama, S. Acetylene-Accelerated Alcohol Catalytic Chemical Vapor Deposition Growth of Vertically Aligned Single-Walled Carbon Nanotubes. *J. Phys. Chem. C* **2009**, *113*, 7511.

34 Sharma, R.; Rez, P.; Treacy, M. M. J.; Stuart, S. J. In Situ Observation of the Growth Mechanisms of Carbon Nanotubes Under Diverse Reaction Conditions. *J. Electron Microsc.* **2005**, *54*, 231.

35 Geohegan, D. B.;A. A.; Puretzky, D.; Styers-Barnett, H.; Hu, B.; Zhao, H.; Cui, C. M.; Rouleau, G.; Eres, J. J.; Jackson, R. F.; Wood, S.; Pannala, J. C. Wells In Situ Time-Resolved Measurements of Carbon Nanotube and Nanohorn Growth. *Phys. Status Solidi B* **2007**, *244*, 3944.

36 Mora, E.; Harutyunyan, A. R. Study of Single-Walled Carbon Nanotubes Growth via the Catalyst Lifetime. *J. Phys. Chem. C* **2008**, *112*, 4805.

37 Moors, M.; Amara, H.; Visart de Bocarme, T.; Bichara, C.; Ducastelle, F.; Kruse, N.; Charlier, J.-C. Early Stages in the Nucleation Process of Carbon Nanotubes. *ACS Nano* **2009**, *3*, 511–516.

38 Harutyunyan, A. R.; Awasthi, N.; Jiang, A.; Setyawan, W.; Mora, E.; Tokune, T.; Bolton, K.; Curtarolo, S. Reduced Carbon Solubility in Fe Nanoclusters and Implications for the Growth of Single-Walled Carbon Nanotubes. *Phys. Rev. Lett.* **2008**, *100*, 195502.

39 Yoshida, H.; Shimizu, T.; Uchiyama, T.; Kohno, H.; Homma, Y.; Takeda, S. Atomic-Scale Analysis on the Role of Molybdenum in Iron-Catalyzed Carbon Nanotube Growth. *Nano Lett.* **2009**, *9*, 3810–3815.

40 Yoshida, H.; Takeda, S.; Uchiyama, T.; Kohno, H.; Homma, Y. Atomic-Scale In-situ Observation of Carbon Nanotube Growth from Solid State Iron Carbide Nanoparticles. *Nano Lett.* **2008**, *8*, 2082–2086.

41 Lin, M.; Ying Tan, J. P.; Boothroyd, C.; Loh, K. P.; Tok, E. S.; Foo, Y.-L. Direct Observation of Single-Walled Carbon Nanotube Growth at the Atomistic Scale. *Nano Lett.* **2006**, *6*, 449–452.